RSC Advances

ROYAL SOCIETY OF CHEMISTRY

www.rsc.org/advances

Fluorescence response of a thiazolidine carboxylic acid derivative for the selective and nanomolar detection of Zn(II) ions: quantum chemical calculations and application in real samples

C. Balakrishnan[a], M. Theetharappan[a], Satheesh Natarajan[b], S. Thalamuthu[a], M.A. Neelakantan[a]*

[a]Chemistry Research Centre, National Engineering College, K. R. Nagar, Kovilpatti 628503, Thoothukudi District, Tamil Nadu, India

[b]Department of Pharmacy, School of Health Sciences, Kwazulu Natal University. Durban-4001, South Africa

*Corresponding Author
Tel: +91 94425 05839, Fax: +91 4632 232749
E-mail Address: drmaneelakantan@gmail.com
maneels@rediffmail.com

Abstract

A thiazolidine carboxylic acid derivative (L) was conveniently synthesized and characterized by spectral techniques and single crystal X-ray crystallography. The complexation of L with zinc (L-Zn^{2+}) was studied by scanning electron microscope (SEM) and energy dispersive spectroscopy (EDS) and further substantiated by ^{1}H NMR and ESI-MS analysis. The L showed excellent specificity and sensitivity towards zinc-induced fluorescence response by forming a 1:1 complex (Job's plot) in 95 % (v/v) water-methanol mixture. The presence of zinc ions causes ~ 40 fold fluorescence enhancement at 481 nm (quantum yield, $\Phi = 0.19$) and can be detected with naked eye under UV-lamp. The L can detect Zn^{2+} in nanomolar level (13.90 nM) with good tolerance in presence of other interfering metal ions. The reversibility of L-Zn^{2+} complexation was checked by EDTA titration. The maximum fluorescence enhancement by Zn^{2+} binding of L was observed in the pH range 7.0–9.0. The dissociation constants of L and stability constant of L-Zn^{2+}complex in 0.15 M $NaClO_4$ were determined by pH metrically. Theoretical calculations were done using density functional theory (DFT) to support the above findings. The L was successfully applied for determination of Zn^{2+} in water samples. The compound (L) detects the presence of, *klebsiella pneumoniae* and *E.coli* in water samples.

Introduction

Sensor is a molecule, which binds the target molecule selectively and produces detectable signal.[1] Heavy metal ions are non-biodegradable and can pollute the biosphere.[2] Hence, the design and synthesis of organic ligands as new sensor materials for heavy and biologically relevant metal ions through changes in fluorescence are of growing interest. Zinc is the second most abundant metal ion in the human body and the cellular biochemistry of Zn^{2+} is diverse and far ranging.[3] The coordinated Zn^{2+} ions are necessary for the function of proteins involved in vital life processes, such as DNA replication and repair, gene expression and cellular metabolism. It is believed that lack of zinc ions can result in an increased risk of several diseases such as stature, mental retardation and digestive dysfunction.[4] Disorders in Zn^{2+} metabolism have been linked to several severe neurological diseases, including Alzheimer's disease, cerebral ischemia, and epilepsy.[5] Insufficiency of micronutrient zinc can lead to impaired cognition, immune dysfunction, diarrhea, and death, particularly in children under the age of 5 years.[6] The accumulation of Zn^{2+} ions in cells leads to death.[7] In addition, high levels of Zn^{2+} ions in water lead to environmental problems. The excessive concentration of zinc in the environment may reduce the soil microbial activity causes phytotoxic effect.[8] Therefore, it is essential to get an insight into the essential roles of Zn^{2+} in biological processes resulting in great demand concerning the design and development of sensors that can selectively and sensitively detect Zn^{2+} in living systems.

Zn^{2+} has $3d^{10}4s^{0}$ electronic configuration and does not produce spectroscopic or magnetic signal. Therefore the presence of Zn^{2+} in samples cannot be measured by common spectral techniques. Some time-consuming and costly instrumentation techniques such as inductively coupled plasma mass spectroscopy (ICP-MS) and atomic absorption spectroscopy (AAS)[9] are currently used to detect zinc ions. Compared with these instrumentation techniques, fluorescent chemosensors are simple, selective, sensitive, low cost and reusable. Zinc forms fluorescent complexes with a variety of organic molecules. These factors thus triggered for the evolution of new class fluorescent sensors for zinc. Though a number of fluorescent sensors for Zn^{2+} have been studied[10-12,25c], the research to develop small organic molecules as fluorescent sensors to detect Zn^{2+} in environmental and biological systems in the occurrence of probable challenging cations like Cd^{2+} is extremely significant.[13] Small-molecule fluorescent sensors sense the metal

ions as (i) intensity-based probes (Zn^{2+} binding induces an increase in fluorescence intensity) or (ii) ratiometric probes (Zn^{2+} binding shifts the excitation and/or emission wavelength). The majority of small molecules are under the category of intensity-based probes operate on the principle of photo induced electron transfer (PET) between the small molecule and the metal binding group.[14]

Biomolecules such as amino acids, peptides, and DNA have been used as a receptor for fluorescent chemosensors because these molecules have strong binding affinities to precise metal ions, biological compatibility.[15] Bacterial pathogens cause infections in humans and animals at the molecular level. For health and safety reasons, the detection of pathogenic bacteria is of great importance. The commonly used methods for the detection of pathogen are cell culture and colony counting[16], PCR-based methods[17,18] and immunological methods (ELISA).[19] The main concern of these methods is the time required for the analysis. Biosensors are developed with the objective of reduced time of analysis in pathogen detection.[20]

Thus in the present work, we demonstrate the design, synthesis and sensing behavior of a novel thiazolidine carboxylic acid derivative, which shows extreme selectivity and sensitivity for Zn^{2+} through the formation of fluorescent L-Zn^{2+} complex. The recognition of Zn^{2+} by L has been investigated by absorption spectroscopy and emission spectroscopy. The complexation of L with zinc was studied by scanning electron microscope (SEM) and energy dispersive spectroscopy (EDS) and further substantiated by ^{1}H NMR and ES-MS analysis. This paper also presents results of a study on protonation equilibria of L and its complexation to Zn^{2+} ions in water methanol mixture by pH metrically. Density functional theory (DFT) and configuration interaction singles (CIS) have also been used to understand the mechanism through which L recognizes the zinc ions. Moreover, practical applications of the L have been discoursed by testing the concentration of Zn^{2+} ions in real samples such as water. As the compound enhances the fluorescence intensity of gram (-ve) bacteria *klebsiella pneumoniae* and *Ecoli*, the detection of bacteria in water samples was also tested.

Results and discussion

Synthesis and general aspects

The compound L was synthesized as reported in our earlier work.[21] In the present work, we were able to isolate the single crystals of L and the structure was characterized by spectral techniques (Fig. S1 – S4) and confirmed by single crystal XRD. The formation of L and its zinc complex is evidenced by spectroscopic and SEM/EDAX data (Fig. 1). The UV-vis spectrum of L shows a distinct band at 285 nm corresponds to π– π * transition.

Crystal structure of L

The atom numbering scheme and the thermal ellipsoid plot of L drawn at 50% probability level using ORTEP[22] is given in Fig. 2. The crystal data and experimental details are listed in Table 1. The structure of L is trigonal units plus oxygen, hydrogen and nitrogen in interstitial positions with the space group *P*3. The atoms C7 [N(1)-C(7)-S(1), N(1)-C(7)-C(6)] and C8 [N(1)-C(8)-C(9), N(1)-C(8)-C(13)] are chiral in nature with the bond angles 110.1(8), 114.9(9), 101.5(7) and 115.5(11) respectively. The sulfur atom, S1 [S(1)-C(9)-C(8)-N(1), N(1)-C(7)-S(1)-C(9) and C(6)-C(7)-S(1)-C(9)] is present at the opposite side of the nitrogen atom (N1) with the torsion angles 49.7(8), 19.7(8) and 145.3(6) respectively. The selected bond lengths, bond angles and symmetry codes of L are given in Table S1.Crystal packing viewed along *b* axis is depicted in Fig. S5.

Absorption spectral studies

The sensing behavior of L was determined by monitoring its UV-visible spectral changes (Fig. 3) in the presence of different metal ions (Fe^{2+}, Ni^{2+}, Mn^{2+}, Hg^{2+}, Ag^{+}, Zn^{2+}, Co^{2+}, K^{+}, VO^{2+}, Cu^{2+}, Cd^{2+}, Fe^{3+}, Na^{+}, Ca^{2+} and Pb^{2+}). The absorption band at 285 nm is due to the π- π* transition of aromatic chromophore of L. Upon addition of different metal ions to L in 95 % (v/v) water-methanol mixture, only in the presence of Zn^{2+} the band at 285 nm undergoes dramatic change in intensity and the new band appeared at 375 nm (Fig. 3). This indicates that L has a pronounced selectivity towards Zn^{2+} ions over the other metal ions screened. The stoichiometry and association constant due to complexation between L and Zn^{2+} were determined using Benesi–Hildebrand (B–H) relationship from the absorbance spectral data with an incremental addition of Zn^{2+} ion (0-100 μM) (Fig. S6). The absorption titration curve fits in a linear 1:1 binding model. The association constant of the L-Zn^{2+} complex is found to be 5.26×10^{5} M^{-1} (±2.5%). This is further supported by the ESI-MS spectral studies of L and its zinc complex (Fig.

S3 and S4). The molecular-ion peak observed at m/z for the zinc complex is attributed to molecular ion [L-Zn^{2+}].

Emission study

The fluorescence response behavior of L was examined upon treatment with various metal ions in 95 % (v/v) water-methanol mixture (Fig. 4a). Among the metal ions, selectively Zn^{2+} ion showed effective fluorescence enhancement under UV light and that can be detected by naked eye (Fig. 4b). The addition of other relevant metal ions, such as Fe^{2+}, Ni^{2+}, Mn^{2+}, Hg^{2+}, Ag^{+}, Zn^{2+}, Co^{2+}, K^{+}, VO^{2+}, Cu^{2+}, Cd^{2+}, Fe^{3+}, Na^{+}, Ca^{2+} and Pb^{2+} caused insignificant fluorescence change even with excess addition. The emission spectrum of L shows almost negligible emission at 481 nm with an excitation of 395 nm. On the addition of different metal ions, only Zn^{2+} ions exhibits ~40 fold enhancement of the fluorescence intensity at 481 nm with a 20 nm red-shift of the emission maxima (Fig.S13). The binding of sensor with metal ion can change the electronic structure and hence fluorescence is energy transfer or electron transfer between the metal and photoexcited probes. Both processes lead to either a fluorescence quenching or enhancement. Weak fluorescence of the present probe (L) is due to the free electrons of the -NH group in the thiazolidine, which can quench the fluorescence of L through photo induced electron transfer (PET). The efficient relaxation pathway developed due to PET decreases the quantum yield of the fluorophore. The binding of zinc ion with electron-rich chelating moiety (L) shifts the charge density and quenches the PET decay pathway and increasing the quantum yield.[23] The fluorescence quantum yield of L-Zn^{2+} determined is found to be 0.19, whereas the fluorescence of the free ligand is insignificant (0.09) (Fig. S7). This demonstrates that an enhancement in quantum yield can be achieved in the complexation of L with Zn^{2+}. The fluorescence enhancement may be due to the electron transfer within a self contained fluorophore−chelate unit upon metal binding. Upon binding Zn^{2+}, photo-excitation of an electron from the highest occupied molecular orbital (HOMO) to the lowest unoccupied molecular orbital (LUMO) leads to a longer-lived excited state and thus fluorescence occurs. That is Zn^{2+} chelation with L decreases the loss of energy through non-radiative transition and leads to fluorescence enhancement.

The association constant value of L-Zn^{2+} was determined from the emission intensity data following the modified Benesi-Hildebrand equation (Fig. S8). From the results the association

constant of the L-Zn^{2+} complex is 2.48 x10^5 M^{-1}. The binding mode between L and Zn^{2+} was determined by using Job plot analysis. As shown in Fig. S9, the Job plot for the L-Zn^{2+} complex exhibited 1:1 stoichiometry. For the realistic applications, the detection limit is a significant parameter. Thus, the detection limit of L for the analysis of Zn^{2+} calculated is 13.90 nM, on the basis of 3σ/*K* (Fig. S10)[24] and is compared with other reported sensors (Table S1).[25] The sensible applicability of L as a selective fluorescence sensor for Zn^{2+} over other metal ions was examined by competition experiments. Upon the addition of 1.0 equivalent of Zn^{2+} in the presence of other metal ions (Fe^{2+}, Ni^{2+}, Mn^{2+}, Hg^{2+}, Ag^{+}, Zn^{2+}, Co^{2+}, K^{+}, VO^{2+}, Cu^{2+}, Cd^{2+}, Fe^{3+}, Na^{+}, Ca^{2+} and Pb^{2+}) the emission intensity of L-Zn^{2+} system was not quenched (Fig. 5). The results show that other metal ions could not interfere in the interaction between L and Zn^{2+}. Therefore, L is a specific Zn^{2+} sensor and be useful in real sample analysis.

In addition, the reversibility studies were also carried out. To study the reversibility of L towards Zn^{2+}, EDTA was added to the solution of L and Zn^{2+} (1:1). The results show that the fluorescence intensity of L-Zn^{2+} was quenched after the addition of EDTA, which indicates regeneration of the free L. Upon a further addition of Zn^{2+} into the mixture solution, the emission intensity was recovered to the original intensity of the L-Zn^{2+} complex (Fig. 6). These results show that L could be recyclable through treatment with suitable reagents such as EDTA.

NMR titration

In order to determine the binding mode of L with Zn^{2+}, the ^{1}H NMR titration was carried out by gradually adding Zn^{2+} ion to DMSO-d_6 solution of L. Changes in the ^{1}H NMR spectra of L before and after the addition of Zn^{2+} are shown in Fig. 7a. The ^{1}H NMR spectrum of the free L showed a broad weak signal at 9.35 ppm which corresponds to the thiazolidine N–H proton. During the addition of Zn^{2+}, this signal is shifted to downfield region indicating that the thiazolidine nitrogen is involved in coordination with metal ion. The L exhibits two isomers arise from two chiral centers at the thiazolidine ring (C2 and C4).[21] ^{1}H NMR spectrum of L shows two sets of signals for each proton (C2 and C4) due to the presence of two isomers with a ratio of 3:2. The chiral proton at C2 and C4 position of thiazolidine ring of the two isomers gives two set of signals at 5.77 and 5.88 ppm and 3.59 and 3.63 ppm, respectively (Fig. 7b). Upon addition of 1.5 equivalents Zn^{2+} to L solution, the signals corresponds to chiral proton at C2 is shifted to 5.78

and 5.93 ppm (downfield shift) and chiral proton at C4 is shifted to 3.67 and 3.65 ppm. These results confirm that Zn^{2+} coordinate to the L.

Effect of pH

The effect of pH on the fluorescence response of L in the absence and in the presence of Zn^{2+} was investigated and the results are illustrated in Fig. 8. The pH of solution was adjusted by either $HClO_4$ or NaOH and fixing the Zn^{2+} concentration at 1×10^{-4} mol L^{-1}. These experiments were carried out at a pH range from 2.0 to 11.0. As it is seen from Fig. 8, the fluorescence intensity increases with increasing pH of solution and reaches a maximum value at pH 7.0. At 7.0 < pH< 8.5, L-Zn^{2+} is strongly fluorescent and then decreases. The ligation of L with Zn^{2+} can be conveniently interpreted from the curve describing the fluorescence variation as a function of pH. The metal - ligand coordination of Zn^{2+} and L occurs through the thiazolidine nitrogen, phenolic oxygen and carboxylato oxygen atoms. The decreased intensity at lower pH might be due to the protonation of the nitrogen atom, –OH and –COOH of L, and cannot bind with the metal center. On the other hand, the reduced optical response of the sensor at pH > 9.0 could be due to the hydroxide formation of zinc ions, resulting in decreased concentration of free Zn^{2+} ions in sample solution. These results demonstrate that L possesses strong fluorescence response towards Zn^{2+} ions in the pH range of 7.0–9.0. Thus, a solution of pH 7.5 is used for further studies.

Protonation and metal complex equilibria

The protonation constants (log K_{LHx}) of L and the corresponding stability constant (log β_{ZnLx}) for the formation of the zinc complex (I = 0.15 M $NaClO_4$) over a wide range of pH (1.8 < pH < 11.5) were determined by analyzing the pH measurements using MINIQUAD-75 program.[26] The L has three protonation centers, viz., phenolic –OH, thiazolidine –NH and carboxylic –COOH groups. The three protonation constants determined are listed in Table S2. Among the three centers the phenolic –OH group is the most basic and its pK value determined is 10.93. The pK value of 6.34 for L corresponds to the protonation of the secondary nitrogen, whereas the value of 2.79 evidently relates to the –COOH group. The pK of 6.34 determined for thiazolidine nitrogen compares well with the value reported earlier.[27] From the species distribution diagram (Fig. 9a), it is clear that $[H_3L]^+$ occurs only at very low pH. The first proton of $[H_3L]^+$ is

completely released at about pH 4.0 from the carboxylic acid moiety. The next deprotonation step occurs at pH 6.0 likely at thiazolidine –NH. The deprotonation of phenolic –OH starts at pH 9.5. The Zn^{2+} binding ability of L was investigated by pH-metry performing the experiments in the 2.0–11.0 pH range. The evaluation of pH-metric titration data led to the speciation model and the overall formation constant is listed in Table S3. The species distribution curve is shown in Fig.9b. The complex formation starts at pH 4.0 by formation of the L-Zn^{2+} complex and is the most prevalent species and reaches the maximum concentration at pH 6.0. This observation indicates that in the [L-Zn^{2+}] complex, the Zn^{2+} is coordinated in a tridentate pocket of the ligand that contains carboxylate -O, thiazolidine –NH and deprotonated phenolic –O donors and fourth position is occupied by a solvent molecule.

DFT analysis

The optimized molecular geometry of L and L-Zn^{2+} complex both in the ground state (GS) and excited state (ES) obtained by employing the DFT/6-31G(d,p) and CIS/6-31G(d,p) method respectively, is depicted in Fig. S11. The selected bond lengths and bond angles of the optimized geometry of L at DFT/B3LYP/6-31G (d,p) level are comparable with the X-ray data (Tables S3 and S4). The results from geometry optimization of the ground and excited states of the L-Zn^{2+} complex shows that the most significant change is the increase in the dihedral angle C(5)-C(6)-C(7)-N(1) leading to a twisted structure (45.29°) in ES from a quite flat conformation (0.72° in GS). Moreover, the dihedral angle C(10)-C(9)-C(8)-N(1) in the thiazolidine ring appears to be a little distorted in ES (171.21°) than in GS (186.19°) as evident from the optimized structures (Tables S5 and S6).

In order to investigate the absorption and emission spectra of L-Zn^{2+} complex, TD-DFT calculation of the optimized GS and ES structures was carried out. The calculated and experimental absorption and emission spectra of the complex and oscillator strength are summarized in Table 2. The calculated absorption λ_{max} differs from the experimental value by 14 nm (Fig. S12) and in the emission spectrum the difference is only 5 nm. The highest occupied molecular orbital (HOMO) and the lowest unoccupied molecular orbital (LUMO) provide information about the electronic properties of the L-Zn^{2+} complex. With respect to L, the HOMO electron density is mainly placed on the thiazolidine unit, while the LUMO electron density is placed on the thiazolidine and phenol units (Fig. 10). But the binding of Zn^{2+} to L, the HOMO

electron density is mainly located on the phenol unit, whereas the LUMO electron density is located on the thiazolidine and phenol units. When compared to L, the energy level of HOMO of L-Zn^{2+} complex increases but the energy level of LUMO decreases. So the HOMO-LUMO energy gap for L-Zn^{2+} complex is smaller than L. These changes can be attributed to the electron redistribution after the binding of Zn^{2+}. Thereby, it indicates that the enhanced fluorescence spectra upon the binding of Zn^{2+} to L, due to changes in the energy level causing by the electron redistribution.

Cell imaging studies

Very few articles in literature report bacterial targeting probes for imaging.[28] In the present investigation we have employed the thiazolidine carboxylic acid derivative (L) as a probe for sensing bacterial cell membranes. Fluorescence micro-plate reader was used to measure the fluorescence resulting from the biosensing assay with excitation at 375 nm and emission at 481 nm. The chemosensor shows high fluorescence enhancements with *Klebsiella pneumoniae* and *E.coli* bacterial cells (Fig. 11). The cell walls contain peptidoglycan, a polymer of N-acetyl glucosamine, N-acetyl muramic acid and amino acids. The fluorescence enhancement with bacterial cells may be due to the formation of ester/amide by the interaction of L containing –OH/–COOH group with the –COOH/–NH_2 groups present in the cell wall of bacteria.

Real sample applications

We have investigated the practical applicability of using L to detect zinc ions in real samples. The analysis was carried out using fluorescence methodology for the detection of zinc ions in water samples (tap water, bore well water and river water). Repeated experiments, checked consistency and the observed results are given in Table 3. The observed results show the practical applicability of L for the detection of Zn^{2+}ions in real samples without any interference from other metal ions. The accuracy of Zn^{2+} detection in different samples is almost quantitative.

Klebsiella pneumoniae and *E.coli* are Gram-negative bacterium found in the normal flora of the mouth, skin, and intestines. Surface water contains *Klebsiella pneumoniae* and *E.coli* has been identified as important common pathogens for nosocomial pneumonia, septicaemia, urinary tract infection and wound infections. To evaluate the practical application of L for the detection of *Klebsiella pneumoniae* and *E.coli*, different water samples were collected from tap water, bore

well water and river water. The bacteria were incubated in these water samples. The results from fluorescence method were compared with plate counting method (Table 4). The results reveal that the proposed compound can be successfully employed as a bacterial detection probe for *Klebsiella pneumoniae* and *E.coli* in water samples.

Conclusion

In summary, we have reported a novel thiazolidine carboxylic acid derivative for the highly sensitive detection of Zn^{2+} ions over other metal ions. Zn^{2+} was able to enhance the fluorescence intensity of L by 40 fold with quantum yield, $\Phi = 0.19$. The fluorescence intensity of the L-Zn^{2+} system can effectively be reversed by the addition of EDTA. The fluorescence can be detected with naked eye under UV-lamp with a low detection limit of 13.90 nM. The binding mode of the metal complex (1:1) was established by combined ^{1}H NMR and ESI-MS and supported by Job's plot. The formation of L and its zinc complex is evidenced by SEM/EDAX data. The dissociation constants of L and stability constant of L-Zn^{2+} complex were determined. Computational calculations using DFT/TD-DFT and CIS/TD-DFT methods confirmed the binding mode and spectral characteristics. Finally, the sensor ability of L towards Zn^{2+} ions was successfully applied in real samples. The results revealed that the compound (L) itself acts as potential sensor for *klebsiella pneumoniae* and *E.coli* in water samples.

Experimental section

Materials and Instrumentation

D-penicillamine, 3-methoxy salicylaldehyde, metal salts and 2-[[1,3-dihydroxy-2-(hydroxymethyl)propane-2-yl]amino] ethane sulphonic acid (TES) were purchased from Sigma Aldrich (USA) and used as received. The spectral grade solvent methanol was purchased from Merck, India. Other commercially available solvents were purified and dried according to the method described elsewhere.[29] Double distilled water was used throughout the experiment. The solutions of metal ions such as Fe^{2+}, Ni^{2+}, Mn^{2+}, Hg^{2+}, Ag^{+}, Zn^{2+}, Co^{2+}, K^{+}, VO^{2+}, Cu^{2+}, Cd^{2+}, Fe^{3+}, Na^{+}, Ca^{2+} and Pb^{2+} were prepared from their chloride and nitrate salts. NMR spectra (400 MHz) were recorded on a Bruker AMX-400 spectrometer using tetramethylsilane as internal standard and DMSO-d_6 as solvent. ESI-MS were obtained using Waters UPLC-TQD mass spectrometer. FT-IR spectra were measured on a Shimadzu-8400 spectrometer with samples

prepared as KBr discs. UV-vis spectra were recorded on a Shimadzu-2450 spectrophotometer using quartz cell with 1 cm path length. The fluorescence spectra were recorded on a JASCO spectrometer at a scan rate of 1000 nm/min and slit width with Ex: 5 nm, Em: 5 nm. SEM/EDS analysis was performed for surface morphology of L and L-Zn^{2+} using a JEOL JSM-5610 SEM equipped with EDS.

Synthesis of L

The compound L was reported in our earlier work.[21] 0.1491g of D-penicillamine (1.0 mM) and 0.1522 g of 3-methoxy salicylaldehyde (1.0 mM) was dissolved in methanol/water mixture (30 mL) and refluxed for two hours. The resulting solution was kept at room temperature in closed condition for a month. In the present investigation, we successfully isolated the single crystals. The colorless crystals were collected by filtration, washed with acetone and dried under vacuum.

Anal. Calcd. for $C_{13}H_{17}NO_4S$ (%): C, 55.11; H, 6.05; N, 4.94; S, 11.32. Found (%): C, 55.32; H, 6.24; N, 5.01; S, 11.45. IR data (KBr, cm^{-1}): (s = strong, m = medium, b = broad). 3400 - 2700 (b) [υ(OH)]; 1635 (s) [υ_{asym}(COO-)], 1369 (s) [υ_{sym}(COO)]; 1354 (m) [υ(OH)]; 1247 (s) [υ(C–O)]; 833 (w) [υ(C–S–C)]; ^{1}H NMR (400 MHz, DMSO-d_6, ppm): 1.62 (singlet (s), CH_3, 3H), 1.31 (singlet (s), CH_3, 3H), 3.38 (singlet, –CH–COOH, 1H), 6.69 - 6.92 (multiplet, aromatic H, 3H), 3.84 (singlet, 3H, -O-CH_3), 5.79 (singlet, thiazolidine –CH–NH, 1H). Color: white. M.p. 143°C; Yield: 73%.

X-ray diffraction studies

Single crystal X-ray diffraction measurements were performed on a Bruker AXS Kappa Apex II CCD Diffractometer equipped with graphite monochromated M_oK_α (λ = 0.71073 Å) radiation at 293(2) K. The structure was solved by direct method procedure using SHELXS-97 program.[30] The refinement was carried out using full matrix least square method on F^2. The geometrical parameters were obtained using PARST[31] and SHELXL-97. The non-hydrogen atoms were refined with anisotropic displacement parameters. The hydrogen atoms bonded to carbon were inserted at calculated positions using a riding model. Hydrogen atoms bonded to oxygen were located from difference map and allowed to refine with temperature factors riding on those of the carrier atoms.

Metal sensing analysis

The test solution containing equimolar concentration of L and metal ions (M, 1:1) was prepared by the following procedure. The stock solutions of various metal ions (5 mL, 0.01 M) were prepared in double distilled water. Stock solution of L (5 mL, 1 mmol) was prepared in 95 % (v/v) water-methanol mixture. The test solutions were prepared by adding 100 μL of stock solution of L into each glass bottle containing 100 μL of individual (M) ion stock solution. Then the solution was diluted to 5 mL with distilled water. After mixing the solutions properly, the UV-vis spectra and emission spectra were taken for each sample at room temperature. For emission measurements, the excitation wavelength was set at 375 nm and emission was recorded from 400 to 650 nm. UV-vis and emission titration were also carried out by keeping the same concentration of L (20 μM) and varying the zinc ion concentration from 0.0 – 3.0 equivalents. Competition experiments were performed in the presence of Zn^{2+} mixed with various metal ions in the ratio of 1:1:2 of L:Zn^{2+}:M.

pH metric measurements

The pH titrations were carried out in a digital pH meter (Systronics μpH System 361) at 310 K with a combined glass electrode (accuracy ± 0.01 pH unit). The instrument was calibrated using standard buffer solutions.[32] The electrode system was calibrated in terms of hydrogen ion concentrations in both the acidic and alkaline regions. The ionic strength of each solution was adjusted to 0.15 M with $NaClO_4$ as the supporting electrolyte. The ion product of water (K_w = $[H^+]$ $[OH^-]$) at 0.15 M $NaClO_4$ in 95 % (v/v) water-methanol mixture was calculated based on the measurement of $[H^+]$ and $[OH^-]$ and pH in several experiments.[33] Oxygen-free nitrogen gas was bubbled through the solution before and during titrations. Multiple titrations were carried out for each system. The dissociation constants (pK_a) of L were obtained from its solutions of concentration ranging from 1.0 x10^{-3} to 3.0 x 10^{-3} M. In zinc:ligand system 25 mL solutions containing low concentration of zinc perchlorate and the ligand (1:1, 1:2, and 1:5) were used. The pK_a and stability constant (log β) values were evaluated with the aid of the MINIQUAD-75 program.[26] The concentration distribution profiles were obtained[34] with HYSS.

Computational details

The ground state geometries were optimized employing Density Functional Theory using Gaussian 03 program[35] suite at the B3LYP level with the standard basis set, 6-31G(d,p) for L and the LANL2DZ effective core potential for L-Zn^{2+}. The optimized structure of L agrees well with the single crystal X-ray diffraction structure. All the structures corresponding to true minima of the potential energy surface were confirmed by the vibrational frequency calculations. The excited state geometry of L and L-Zn^{2+} were optimized by configuration interaction singles CIS/6-31G(d,p) method. The TD-DFT method was employed to optimize the first excited state (S_1) geometries without constraint by using the ground equilibrium geometries. The absorption and emission spectra calculated using the TD-DFT method agrees with the results obtained from the experimental studies.

Real samples preparation

Water samples were tested in the present investigation. The practical applicability of L to detect zinc ions in real water samples was tested in tab water, bore water and river water. Fifteen water samples were collected from local area and diluted with buffered solution in a 25.0 ml volumetric flask. Insoluble materials present in the samples were removed by filtration. The initial concentration of Zn^{2+} in the samples was determined by AAS. Then different amounts of Zn^{2+} were added to each water sample and were tested by fluorescence method and AAS. The detection of Zn^{2+} in water samples in the presence of other metal ions was also carried out.

Bacterial cell culture and fluorescence microscopic study

Bacterial cells were cultured overnight in Luria-Bertani Miller broth and allowed to grow overnight by incubating at 37ºC and a shaker speed of 200 rpm. Cells were harvested by centrifugation at 3500 rpm for 4 min with TES buffer (5 mM TES, 145 mM NaCl, pH 7.4). Cells representing ~10^3concentration were used for the study. The bacterial cells were treated with 10 μM of L and incubated for 30 min at 37°C. A portion of the cells was washed 3 times with TES buffer and immediately mounted on a slide and observed under a fluorescence microscope.

Support Information

Spectra, Jobs plot, association constant and detection limit calculations, optimized geometry and data are given in supporting information. Crystallographic data are deposited with the Cambridge Crystallographic Data Centre: deposition number CCDC 918759 for L. These data can be

obtained free from the Cambridge Crystallographic Data Centre via http://www.ccdc.cam.ac.uk/cgibin/catreq.cgi.

Acknowledgements

Financial supports received from the Council of Scientific and Industrial Research (CSIR), New Delhi, India (01(2736)/13/EMR-II) and Board of Research in Nuclear Science (BRNS), BARC-DAE, Mumbai, India (35/14/03/2014/BRNS) is gratefully acknowledged. C.B. thanks the CSIR for his fellowship. M.T is thankful to BRNS, India for his fellowship.

References

1 (a) H. L. Li, J. L. Fan, J. J. Du, K. X. Guo, S. G. Sun, X. J. Liu and X. J. Peng, *Chem. Commun*., 2010, **46**, 1079–1081; (b) Y. Yang, C. Gao, B. Li, L. Xu and L. Duan, *Sens. Actuators B*, 2014, **199**, 121–126; (c) J. Wang, W. Lin, L. Yuan, J. Song and W. Gao, *Chem. Commun*., 2011, **47**, 12506–12508; (d) H. N. Kim, W. X. Ren, J. S. Kim and J. Yoon, *Chem. Soc. Rev*., 2012, **41**, 3210–3244; (e) B. Annaraj and M. A. Neelakantan, *Anal. Methods*, 2014, **6**, 9610–9615.

2 (a) E. M. Nolan and S. J. Lippard, *Chem. Rev*., 2008, **108**, 3443–3480; (b) A. K. Mandal, M. Suresh, E. Suresh, S. K. Mishra, S. Mishra and A. Das, *Sens. Actuators B*, 2010, **145**, 32–38.

3 (a) A. I. Bush, W. H. Pettingell, G. Multhaup, M. Paradis, J. P. Vonsattel, J. F. Gusella, K. Beyreuther, C. L. Masters and R. E. Tanzi, *Science*, 1994, **265**, 1464–1465; (b) C. J. Frederickson, J. Y. Koh and A. I. Bush, *Nat. Rev. Neurosci.*, 2005, **6**, 449–452; (c) D. D. Mott, M. Benveniste and R. J. Dingledine, *J. Neurosci.*, 2008, **28**, 1659–1671; (d) J. M. Berg and Y. Shi, *Science*, 1996, **271**, 1081–1085. (e) P. J. Fraker and L. E. King, *Annu. Rev. Nutr*., 2004, **24**, 277−298.

4 (a) A. Krężel and W. Maret, J. Biol. Inorg. Chem., 2006, 11, 1049−1062; (b) A. Staszewska, E. Kurowska and W. Bal, *Metallomics*, 2013, **5**, 1483–1490.

5 (a) P.O. Tsvetkov, I.A. Popov, E.N. Nikolaev, A.I. Archakov, A.A. Makarov and S.A. Kozin, *Chem. BioChem*., 2008, **9**, 1564–1567; (b) G. Wei, C.J. Hough, Y. Li and J.M. Sarvey, Neuroscience, 2004, 125, 867–877; (c) J. Kapur and R.L. Macdonald, *J.Neurosci*., 1997, **17**, 7532–7540.

6 M. Hambidge, *J. Nutr.*, 2000, **130**, 1344S–1349S.

7 L.A. Lichten and R. Cousins , *Annu. Rev. Nutr*., 2009, **29**, 153–176.

8 A. Voegelin, S. Poster, A.C. Scheinost, M.A. Marcus and R. Kretzschmar, *Environ. Sci. Technol*., 2005, **39**, 6616.

9 (a) C. V. Banks and R. E. Bisque, *Anal. Chem.*, 1957, 29, 522–526; (b) A. R. Fakhari, M. Shamsipur and K. H. Ghanbari, *Anal. Chim. Acta*, 2002, 460, 177–183; (c) Q. Li, X.H. Zhao, Q. Z. Lv and G. G. Liu, *Sep. Purif. Technol.*, 2007, **55**, 76–81; (d) D. Karunasagar, J. Arunachalam and S. Gangadharan, *J. Anal. At. Spectrom*., 1998, **13**, 679–682. (e) Y. Li, C. Chen, B. Li, J. Sun, J. Wang, Y. Gao, Y. Zhao and Z. Chai, *J. Anal. At. Spectrom*., 2006, **21**, 94–96.

10 (a) K. K. Upadhyay, A. Kumar, J. Zhao and R. K. Mishra, *Talanta*, 2010, **81**, 714–721; (b) J. F. Zhang, S. Kim, J. H. Han, S. J. Lee and J. S. Kim, *Org. Lett.*, 2011, **13**, 5294–5297; (c) Y. Xu, J. Meng, L. X. Meng, Y. Dong, Y. X. Cheng and C. J. Zhu, *Chem. Eur. J.*, 2010, **16**, 12898–12903; (d) Q. H. You, P. S. Chan, W. H. Chan, N. K. Mak and R. N. S. Wong, *RSC Adv.*, 2012, **2**, 11078–11083; (e) H. Y. Lin, P. Y. Cheng, C. F. Wan and A. T. Wu, *Analyst*, 2012, **137**, 4415–4417; (f) T. Gajda, N. Buzas, L. Nagy and K. Burger, *Polyhedron*, 1992, **11**, 2237−2243; (g) T. Gajda, L. Nagy and K. Burger, *J. Chem. Soc., Dalton Trans.,* 1990, 3155−3160.

11 (a) S. Comby, S. A. Tuck, L. K. Truman, O. Kotova and T. Gunnlaugsson, *Inorg. Chem.*, 2012, **51**, 10158–10168; (b) J. Jia, Q. C. Xu, R. C. Li, X. Tang, Y. F. He, M. Y. Zhang, Y. Zhang and G. W. Xing, *Org. Biomol. Chem.*, 2012, **10**, 6279–6286; (c) X. Meng, S. Wang, Y. Li, M. Zhu and Q. Guo, *Chem. Commun.*, 2012, **48**, 4196–4198; (d) T. Mukherjee, J. C. Pessoa, A. Kumar and A. R. Sarkar, *Dalton Trans.*, 2012, **41**, 5260–5271; (e) S. H. Mashraqui, R. Betkar, S. Ghorpade, S. Tripathi and S. Britto, *Sens. Actuators, B*, 2012, **174**, 299–305. (f) Z. Guo, G. H. Kim, I. Shin, J. Yoon, *Biomaterials*, 2012, **33**, 7818−7827; (g) G. Sivaraman, T. Anand and D. Chellappa, *Anal. Methods*, 2014, **6**, 2343−2348; (h) Z. Guo, G. H. Kim, J. Yoon and I. Shin, *Nat. Protoc*., 2014, **9**, 1245–1254.

12 (a) G. Mandal, M. Darragh, Y. A. Wang and C. D. Heyes, *Chem. Commun.*, 2013, **49**, 624–626; (b) G. Sivaraman, T. Anand and D. Chellappa, *Analyst*, 2012, **137**, 5881–5884; (c) L. J. Liang, S. J. Zhen, X. J. Zhao and C. Z. Huang, *Analyst*, 2012, **137**, 5291–5294; (d) P. G.

Sutariya, N. R. Modi, A. Pandya, B. K. Joshi, K. V. Joshi and S. K. Menon, *Analyst*, 2012, **137**, 5491–5494; (e) Y. W. Choi, G. J. Park, Y. J. Na, H. Y. Jo, S. A. Lee, G. R. You and C. Kim, *Sens. Actuators, B*, 2014, **194**, 343–352; (f) E. J. Song, H. Kim, I. H. Hwang, K. B. Kim, A. R. Kim, I. Noh and C. Kim, *Sens. Actuators, B*, 2014, **195**, 36–43; (g) G. J. Park, H. Kim, J. J. Lee, Y. S. Kim, S. Y. Lee, S. Lee, I. Noh, C. Kim, *Sens. Actuators, B*, 2015, **215**, 568–576; (h) J. J. Lee, S. A. Lee, H. Kim, L. T. Nguyen, Insup Noh and Cheal Kim, *RSC Adv.***,** 2015, **5**, 41905-41913; (i) A. K. Bhanja, C. Patra, S. Mondal, D. Ojha, D. Chattopadhyay and C. Sinha**,** *RSC Adv.***,** 2015, **5**, 48997–49005; (j) C.X. Yin, L.J. Qu, F.J. Huo, *Chin. Chem. Lett.*, 2014, **25**, 1230–1234.

13 R. R. Lauwerys, A. M. Bernard, H. A. Reels and J.P. Buchet, *Clin. Chem*., 1994, **40**, 1391–1394.

14 K. P. Carter, A. M. Young and A. E. Palmer, *Chem. Rev.,* 2014, **114**, 4564–4601.

15 (a) L. J. Ma, Y. Li, L. Li, J. Sun, C. Tian and Y. Wu, *Chem. Commun.,* 2008, 6345− 6347; (b) M. H. Yang, C. R. Lohani, H. J. Cho and K. H. Lee, *Org. Biomol. Chem.*, 2011, **9**, 2350−2356.

16 E. Leoni and P.P. Legnani, *J. Appl. Microbiol.*, 2001, **90**, 27–33.

17 A. K. Bej, M. H. Mahbubani, J. L. Dicesare and R. M. Atlas, *Appl. Environ. Microbiol*., 1991, **57**, 3529–3534.

18 A. K. Bej, R. J. Steffan, J. D. Cesare, L. Haff and R. M. Atlas, *Appl. Environ. Microbiol*., 1990, **56**, 307–314.

19 O. Lazcka, F. J. Del Campo and F. X. Munoz, *Biosens. Bioelectron*., 2007, **22**1205–1217.

20 W. M. Leevy, S. T. Gammon, H. Jiang, J. R. Johnson, D. J. Maxwell, E. N. Jackson, M. Marquez, D. P. Worms and B. D. Smith*, J. Am. Chem. Soc*., 2006, **128**, 16476−16477.

21 S. Thalamuthu, B. Annaraj, S. Vasudevan, S. Sengupta and M. A. Neelakantana, *J. Coord. Chem.*, 2013, **66**, 1805–1820.

22 L. J. Farrugia, *J. Appl. Cryst*., 1997, **30**, 565.

23 K. P. Carter, A. M. Young and A. E. Palmer, *Chem. Rev.,* 2014, **114**, 4564–4601.

24 (a) Z. Xu, J. Yoon and D. R. Spring, *Chem. Soc. Rev*., 2010, **39**, 1996–2006.

25 (a) V. K. Gupta, A. K. Singh and L. K. Kumawat, *Sensor Actuat. B-Chem*., 2014, **204**, 507–514; (b) S. H. Mashraqui, R. Betkar, S. Ghorpade, S. Tripathi and S. Britto, *Sensor*

Actuat. B-Chem., 2012, **174**, 299–305; (c) K. Ponnuvel, V. Padmini and R. Sribalan, *Sensor Actuat. B-Chem*., 2016, **222**, 605–611; (d) L. Subha, C. Balakrishnan, S. Natarajan, M. Theetharappan, B. Subramanian and M. A. Neelakantan, Spectrochim. Acta A, 2016, **153**, 249–256; (e) A. J. Sanchez, B. Ortiz, V. O. Navarrete, N. Farfan and R. Santillan, *Analyst*, 2015,**140**, 6031−6039; (f) K. B. Kim, H. Kim, E. J. Song, S. Kim, I. Noh and C. Kim, *Dalton Trans*., 2013,**42**, 16569−16577; (g) M. Hosseini, A. Ghafarloo, M. R. Ganjali, F. Faridbod, P. Norouzi and M. S. Niasari, *Sensor Actuat. B-Chem*., 2014, **198**, 411–415.

26 Z. X. Huang, P. M. May and D. R. Williams, *Inorg. Chim. Acta*., 1981, **56**, 41–44.

27 (a) A. Sabatini, A. Vacca and P. Gans, *Talanta*, 1974, **21**, 53–77; (b) A. Sabatini, A. Vacca and P. Gans, *Inorg. Chim. Acta*, 1976, **18**, 237–239.

28 (a) R. Y. Tsien, *Fluorescent and Photochemical Probes of Dynamic Biochemical Signals inside Living Cells*, ed. A. W. Czarnik, American Chemical Society, Washington, DC, 1993, 130–146; (b) Y. Xiang, A. J. Tong, P. Y. Jin and Y. Ju, *Org. Lett*., 2006, **8**, 2863–2866.

29 A. I. Vogel, *Textbook of Practical Organic Chemistry*, Singapore Publishers Ltd., 5th ed. Singapore, 1994, pp. 397–403.

30 G. M. Sheldrick, SHELXS-97, *Program for the Solution of Crystal Structures*, University of Gottingen, Germany, 1997.

31 M. Nardelli, *J. Appl. Cryst*., 1995, **28**, 659.

32 H. M. Irving, M. G. Miles and L. D. Pettit, *Anal. Chim. Acta*, 1967, **38**, 475–488.

33 M. A. Neelakantan, M. Sundaram and M. Sivasankaran Nair, *J. Chem. Eng. Data*, 2011, **56**, 2527–2535.

34 L. Alderighi, P. Gans, A. Ienco, D. Peters, A. Sabatini and A. Vacca, *Coord. Chem. Rev*., 1999, **184**, 311–318.

35 M. J. Frisch, G. W. Trucks, H. B. Schlegel,; G. E.Scuseria, M. A. Robb, R. J. Cheeseman,Jr. J. A. Montgomery, T. Vreven, K. N. Kudin, J. C. Burant, J. M. Millam, S. S. Iyengar, J. Tomasi, V. Barone, B. Mennucci, M. Cossi, G. Scalmani, N. Rega, G. A. Petersson, H. Nakatsuji, M. Hada, M. Ehara, K. Toyota, R. Fukuda, J. Hasegawa, M. Ishida, T. Nakajima, Y. Honda, O. Kitao, H. Nakai, M. Klene, X. Li, J. E. Knox, H. P.

Hratchian, J. B. Cross, C. Adamo, J. Jaramillo, R. Gomperts, R. E. Stratmann, O. Yazyev, A. J. Austin, R. Cammi, C. Pomelli, J. W. Ochterski,P. Y. Ayala, K. Morokuma, G. A. Voth, P. Salvador, J. J. Dannenberg, V. G. Zakrzewski, S.Dapprich, A.D. Daniels, M. C. Strain, O. Farkas, D. K.Malick, A. D. Rabuck, K. Raghavachari, J. B. Foresman, J. V. Ortiz, Q. Cui, A. G. Baboul, S. Clifford, J. Cioslowski, B. B. Stefanov, G. Liu, A. Liashenko, P. Piskorz, I. Komaromi, R. L. Martin, D. J. Fox, T. Keith, M. A. Al-Laham, C. Y. Peng, A. Nanayakkara, M. Challacombe, P. M. W. Gill, B. Johnson, W. Chen, M. W. Wong, C. Gonzalez and J. A. Pople, Gaussian 03, Revision E.01, Gaussian, Inc.: Wallingford, CT, 2004.

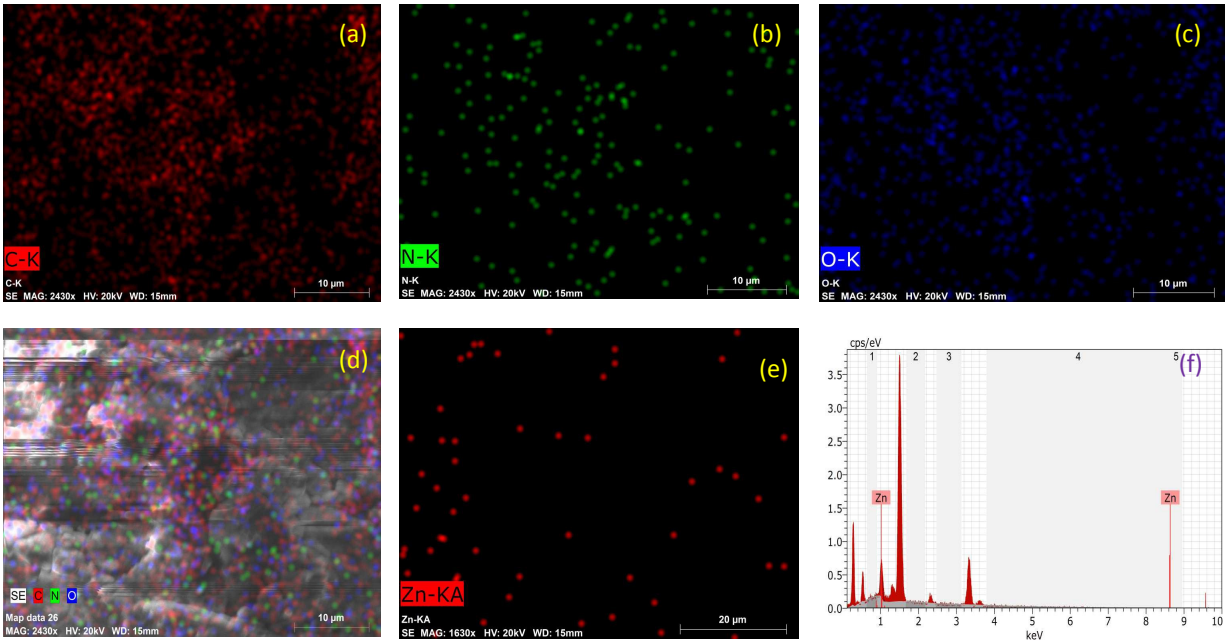

Fig. 1 FE-SEM elemental color mapping image of L and L-Zn^{2+}. For L (a) C, (b) N, (c) O (d) C, N and O; For L-Zn^{2+} (d) Zn, (f) EDS spectra.

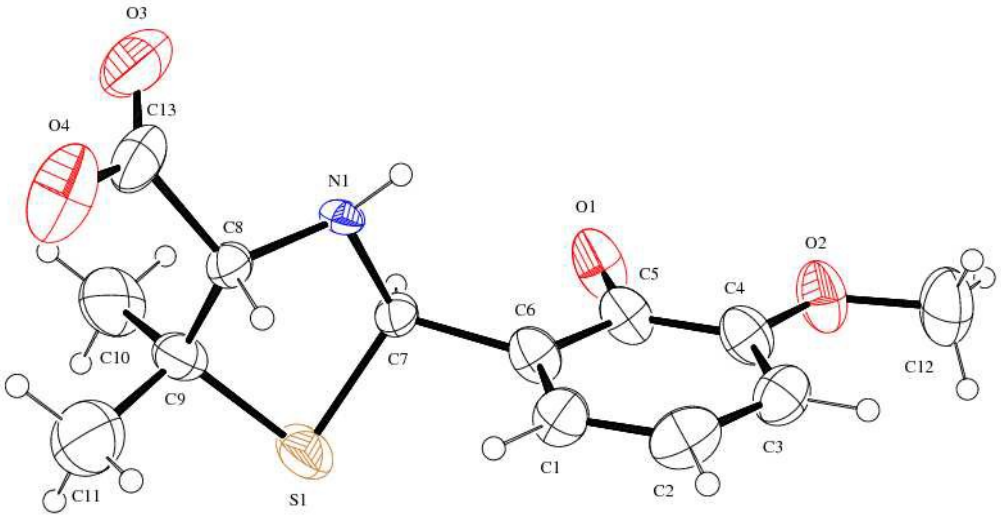

Fig. 2 ORTEP view of ligand L at 50% probability level (CCDC: 918759).

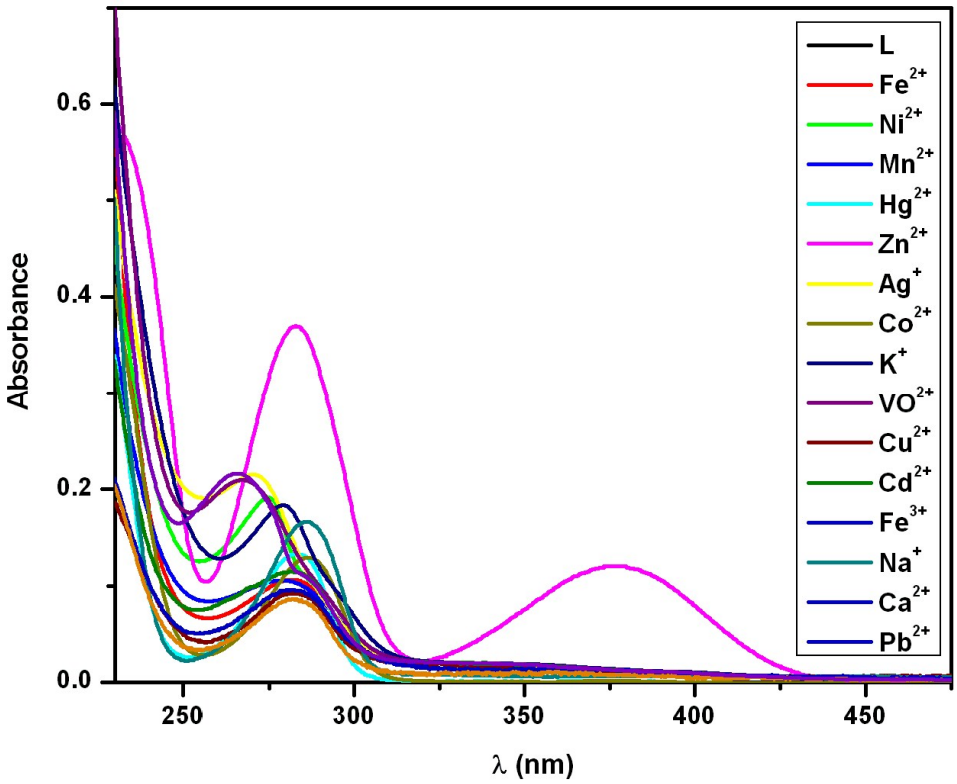

Fig. 3 Changes in absorption spectra of L with different metal ions (Fe^{2+}, Ni^{2+}, Mn^{2+}, Hg^{2+}, Ag^{+}, Zn^{2+}, Co^{2+}, K^{+}, VO^{2+}, Cu^{2+}, Cd^{2+}, Fe^{3+}, Na^{+}, Ca^{2+} and Pb^{2+}) in 95% (v/v) water-methanol mixture.

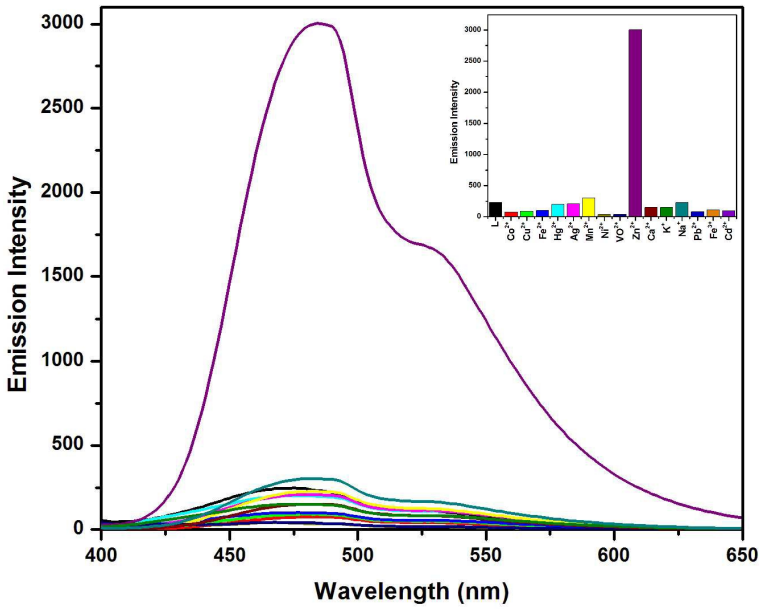

(a)

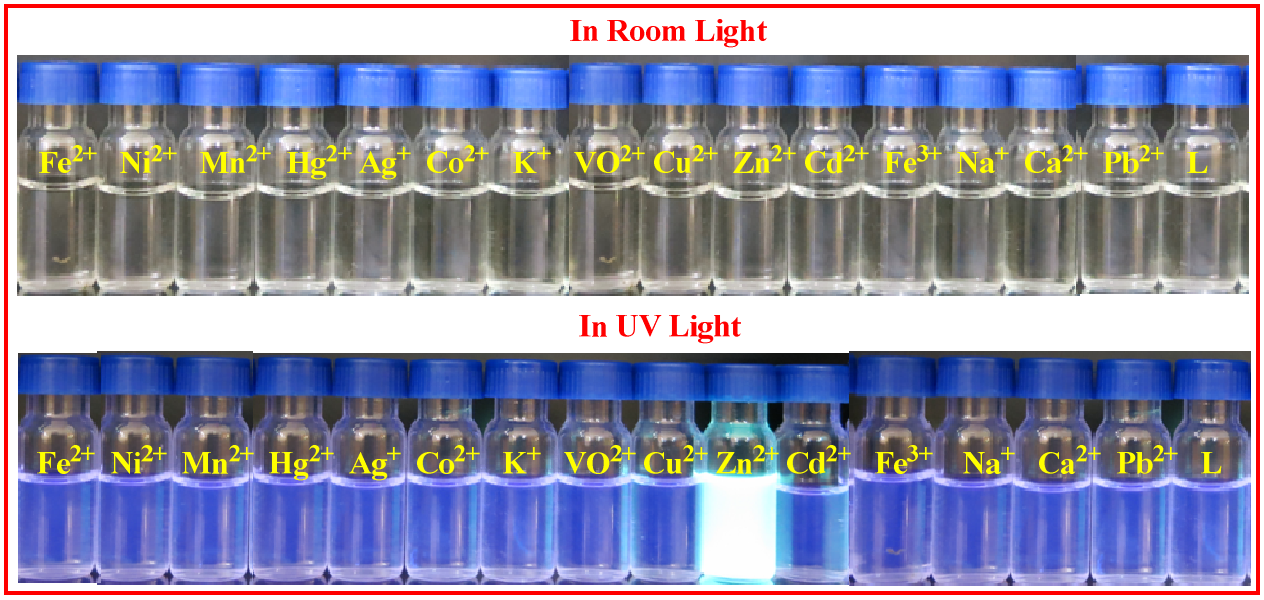

(b)

Fig. 4 (a) Changes in emission spectra of L (10 μM) in the presence of various metal ions; **(b)** Visual color changes of L (10.0 μM) upon the addition of different metal ions in 95 % (v/v) water-methanol mixture (Fe^{2+}, Ni^{2+}, Mn^{2+}, Hg^{2+}, Ag^{+}, Zn^{2+}, Co^{2+}, K^{+}, VO^{2+}, Cu^{2+}, Cd^{2+}, Fe^{3+}, Na^{+}, Ca^{2+} and Pb^{2+}).

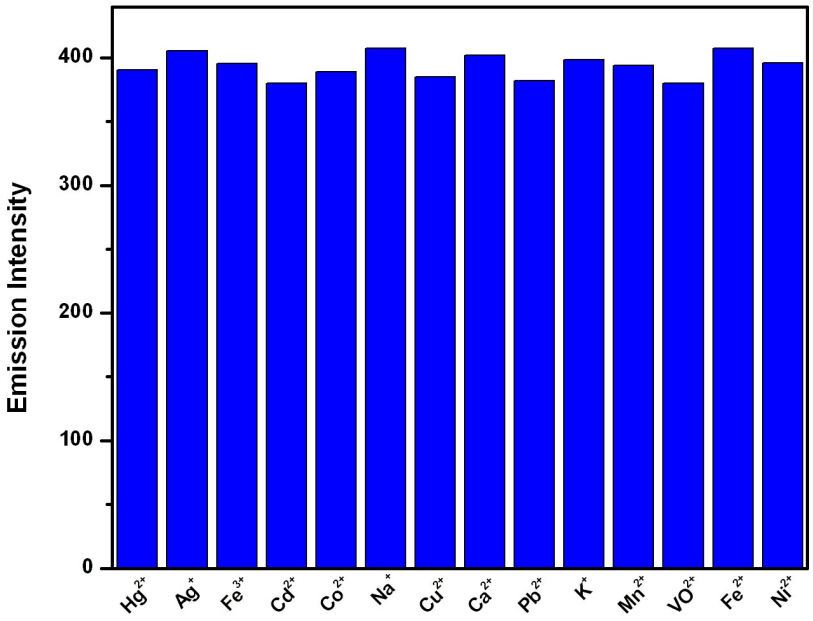

Fig. 5 Competition study using Fluorescence method, after addition of different analytes (Fe^{2+}, Ni^{2+}, Mn^{2+}, Hg^{2+}, Ag^{+}, Co^{2+}, K^{+}, VO^{2+}, Cu^{2+}, Cd^{2+}, Fe^{3+}, Na^{+}, Ca^{2+} and Pb^{2+}) in the solution of L (5 μM) in presence of Zn^{2+} in 95 % (v/v) water-methanol mixture.

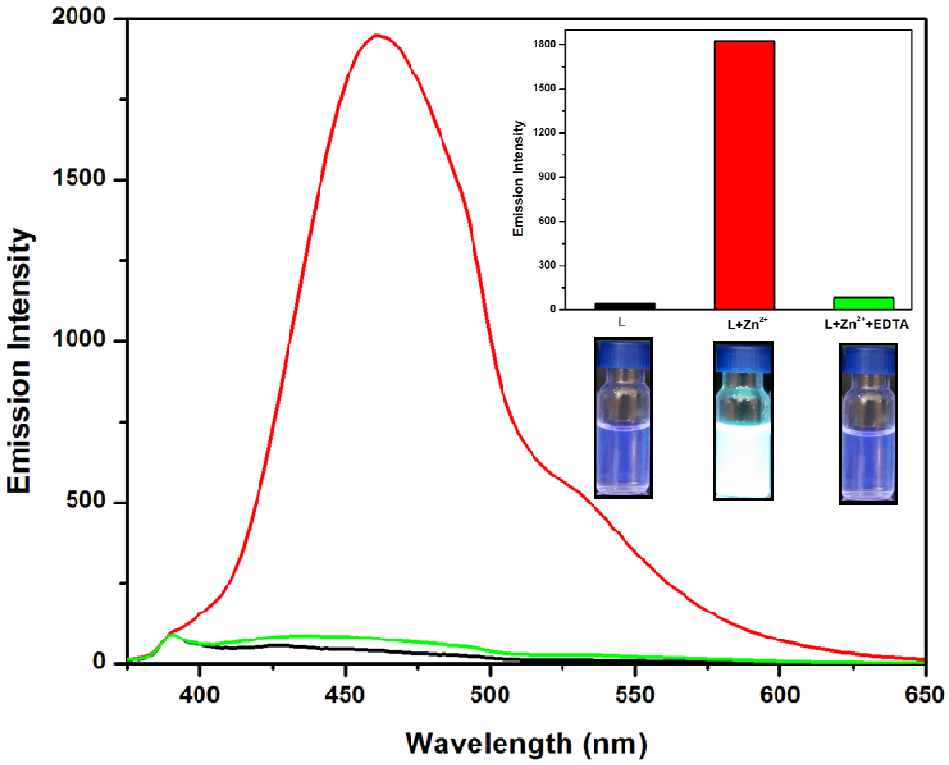

Fig. 6 Fluorescence intensity of L with Zn^{2+} ions and EDTA in 95 % (v/v) water-methanol mixture; Inset: visual fluorescence changes of L with Zn^{2+} ions and EDTA.

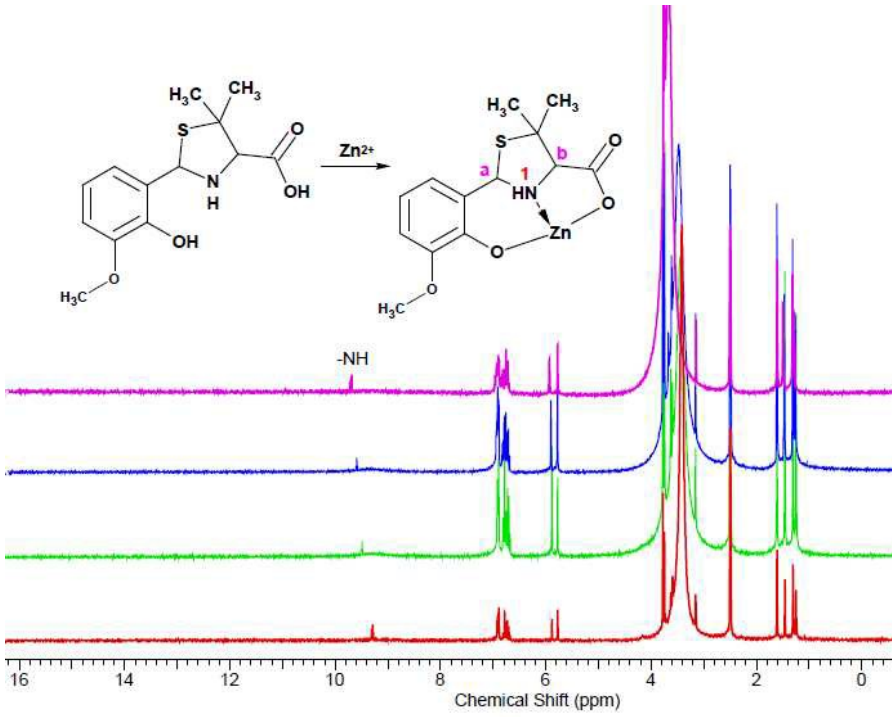

(a)

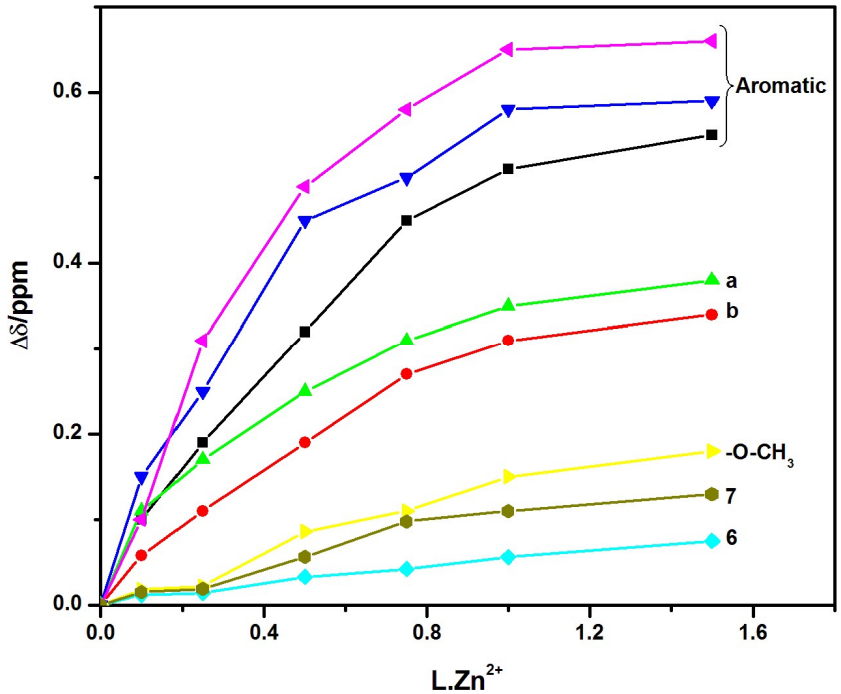

(b)

Fig. 7 (a) ^{1}H NMR spectra of L by stepwise addition of Zn^{2+}; **(b)** ^{1}H NMR titration curves for L with Zn^{2+}.

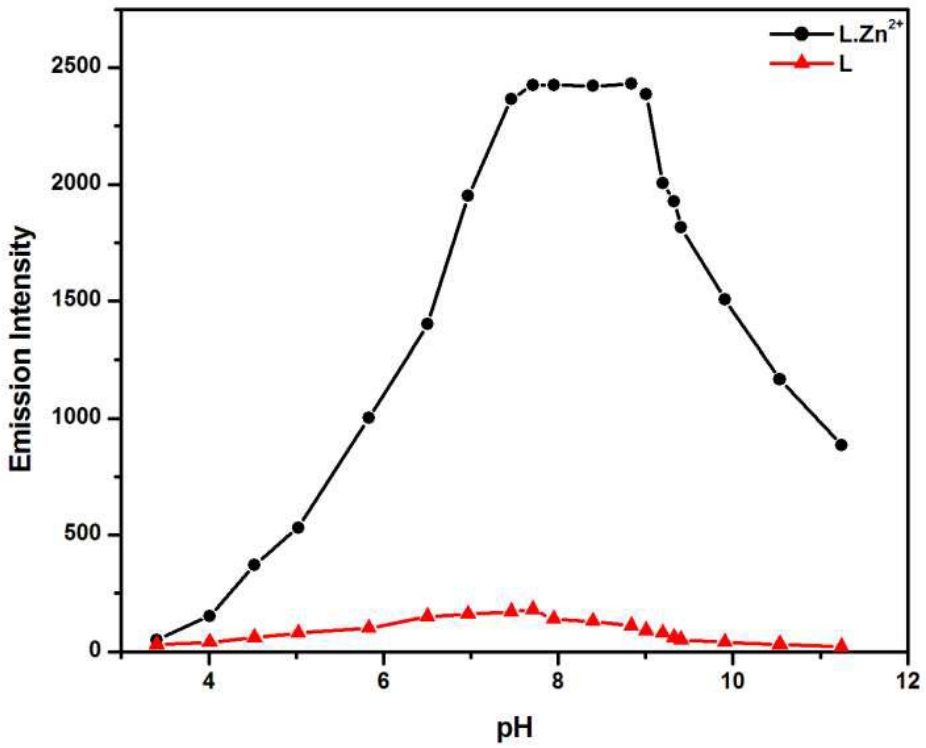

Fig. 8 Fluorescence response of L and L-Zn^{2+} at 481 nm (10 μM) as a function of pH in 95 % (v/v) water-methanol mixture.

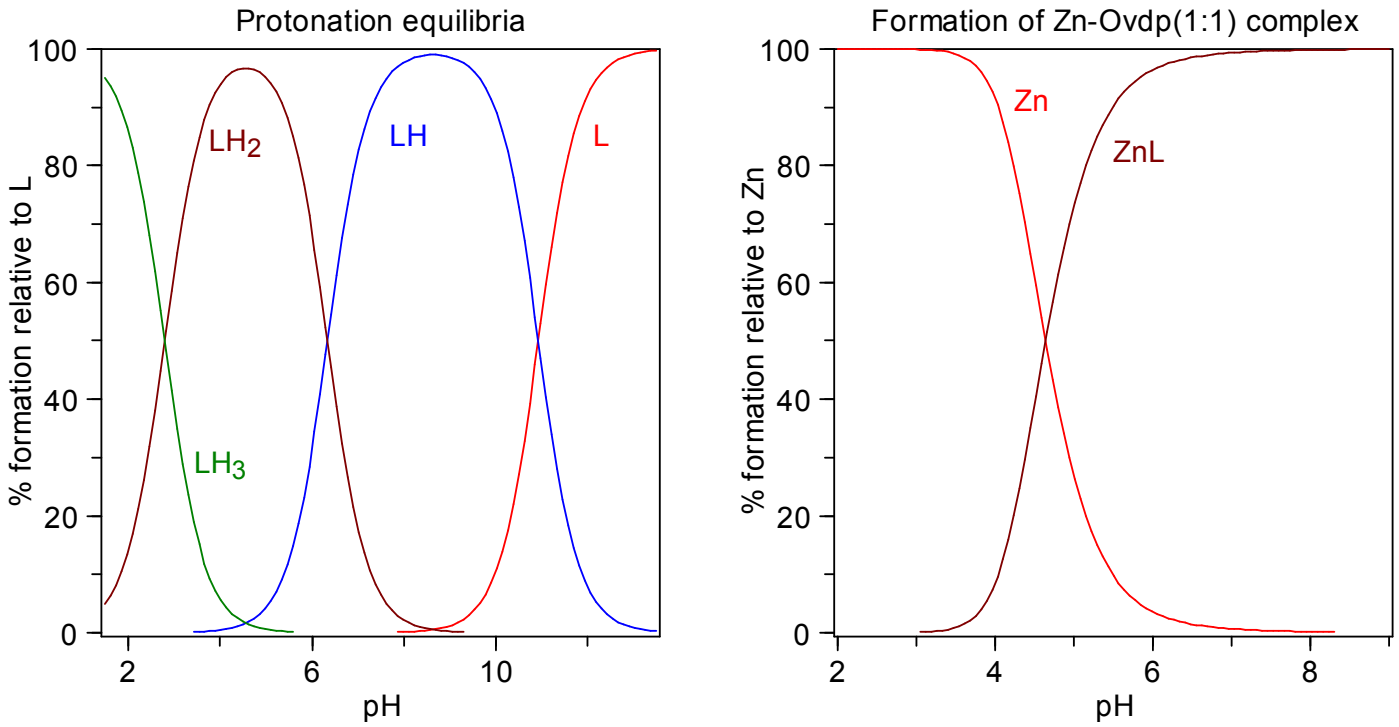

Fig. 9 Species distribution diagram of (a) protonation equilibria of L (C_L=0.003M) and (b) binary L-Zn^{2+} complex equilibria ($C_L = C_M = 0.003$M) in 95 % (v/v) water/methanol mixture.

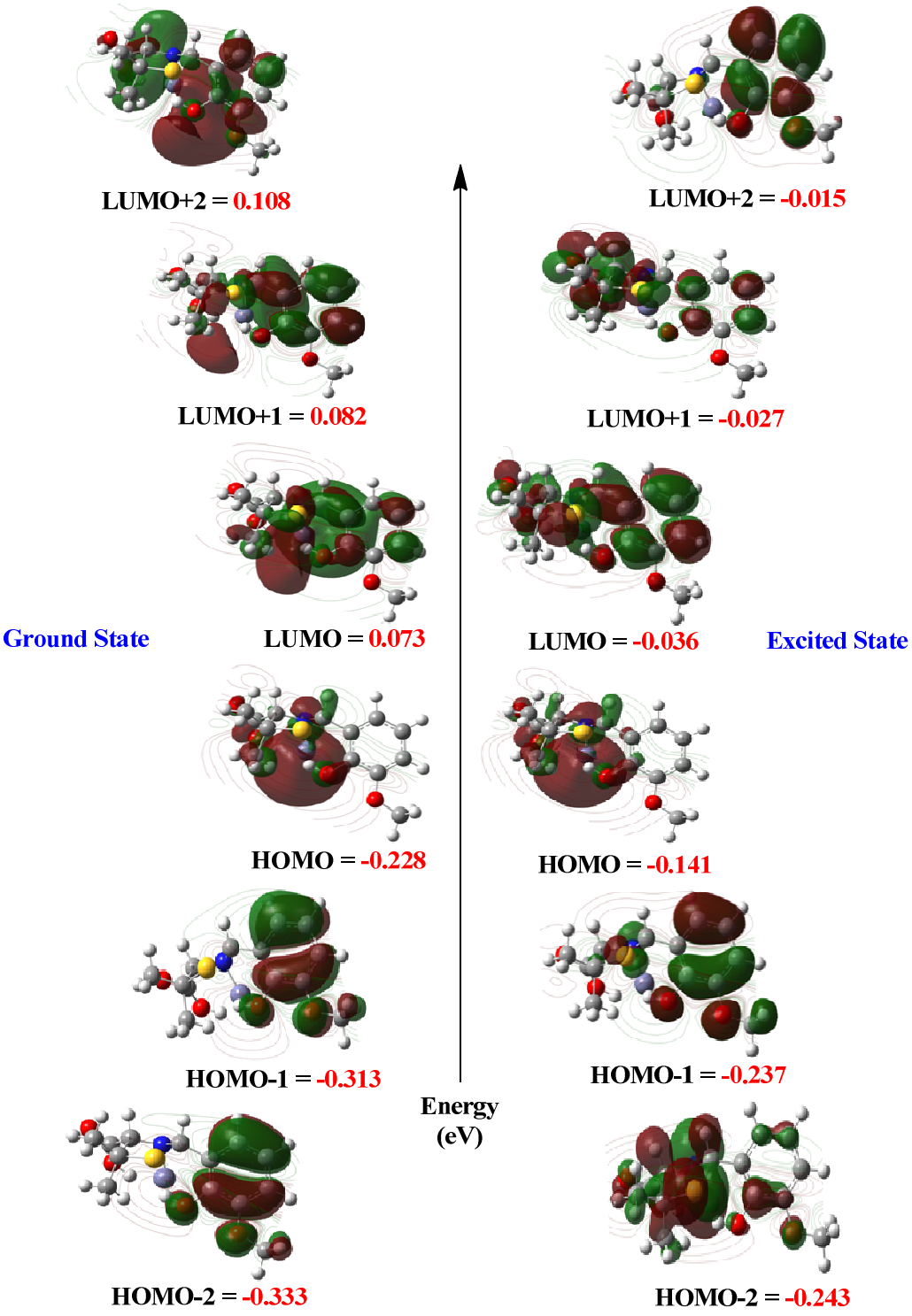

Fig. 10 Frontier molecular orbital diagram of the L-Zn^{2+}complex.

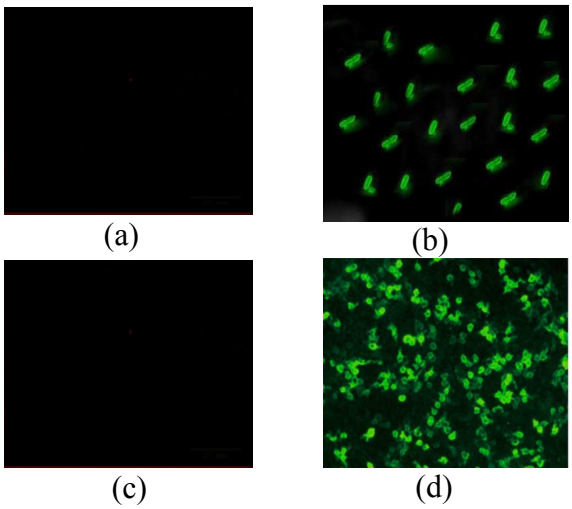

Fig. 11 Fluorescence images of (a) klebsiella pneumoniae; (b) klebsiella pneumoniae treated with L; (c) Ecoli; (d) Ecoli treated with L.

Table 1 Crystal data and structure refinement for L.

Structural parameters	
Empirical formula	$C_{13}H_{17}NO_4S$
Formula weight	293.01
Temperature (K)	293(2) K
Wavelength (Å)	0.71073
Crystal system	Trigonal
Space group	P3
Unit cell dimensions	a = 14.014(2) Å alpha = 90°
	b = 14.014(2) Å beta = 90°
	c = 6.4750(10) Å gamma = 120°
Unit cell Volume (A^3)	1101.3(3)
No. of formula units per unit cell , Z	3
Calculated density	1.325 Mg/m^3
Absorption coefficient	0.233 mm^-1
F(000)	465
Crystal size	0.30 x 0.20 x 0.20 mm
Theta range for data collection	2.91 to 22.83 deg.
Limiting indices	-15<=h<=15, -15<=k<=15, -6<=l<=6
Reflections collected / unique	4700 / 1798 [R(int) = 0.0279]
Completeness to θ = 22.83	99.0 %
Absorption correction	Semi-empirical from equivalents
Max. and min. transmission	0.962 and 0.910
Refinement method	Full-matrix least-squares on F^2
Data / restraints / parameters	1798 / 146 / 253
Largest diff. peak and hole	0.199 and -0.154 ($e.A^{-3}$)
Final R indices [I>2σ (I)]	R1 = 0.0458, wR2 = 0.1072
R indices (all data)	R1 = 0.0542, wR2 = 0.1132
Absolute structure parameter	-0.03(15)
Extinction coefficient	0.036(6)
Goodness-of-fit on F^2	1.046

Table 2 Comparison of λ_{abs} and λ_{em} of L-Zn^{2+} complex along with oscillator strength as observed in experimental and theoretical calculations.

	Experimental	Theoretical	oscillator strength
Absorption	375 nm	389 nm	0.0162
Emission	481 nm	486 nm	0.0317

Table 3 Determination of Zn^{2+} ion in water samples with L.

Sample	Determined by AAS	Added (mol L^{-1})	Found (mol L^{-1})	Recovery (%)
Bore water	8.5 (±0.1) x 10^{-6}	3.0(±0.1) x 10^{-6}	3.1(±0.2) x 10^{-6}	102.3
		5.0(±0.2) x 10^{-6}	5.3(±0.1) x 10^{-6}	104.2
Tap water	2.0 (±0.1) x 10^{-6}	4.0(±0.1) x 10^{-6}	4.2(±0.2) x 10^{-6}	103.8
		5.0(±0.2) x 10^{-6}	5.1(±0.2) x 10^{-6}	102.5
River water	3.5 (±0.1) x 10^{-6}	4.0(±0.1) x 10^{-6}	3.9(±0.1) x 10^{-6}	99.1
		6.0(±0.2) x 10^{-6}	6.1(±0.2) x 10^{-6}	102.8

Table 4 Detection of *klebsiella pneumoniae* and *Ecoli* in water samples using L.

S. No.	Sample	Plate count method (*CFU/200mL)	With L (*CFU/200mL)
	Klebsiella pneumoniae		
1.	Bore water	2.15×10^1	2.18×10^1
2.	Tap water	4.78×10^1	4.85×10^1
3.	River water	3.26×10^3	3.39×10^3
	Ecoli		
1.	Bore water	2.22×10^1	2.31×10^1
2.	Tap water	4.91×10^1	5.11×10^1
3.	River water	3.39×10^3	3.42×10^3

*CFU – Colony Forming Unit